# Structural Changes Induced by Binding of the High-Mobility Group I Protein to a Mouse Satellite DNA Sequence

A. Slama-Schwok,* K. Zakrzewska,† G. Léger,‡ Y. Leroux,‡ M. Takahashi,§ E. Käs,¶ and P. Debey*

*INRA 806/EA2703 Muséum National d'Histoire Naturelle, Institut de Biologie Physico-Chimique, Paris; †Laboratoire de Biochimie Théorique CNRS UPR 9080, Institut de Biologie Physico-Chimique, Paris; ‡Laboratoire de Chimie Structurale Biomoléculaire UPRESA 7031, IFR Biomédicale, Bobigny; §UMR 216 CNRS and Institut Curie, Université Paris-Sud, Orsay; and ¶Laboratoire de Biologie Moléculaire Eucaryote, CNRS UPR 9006, Toulouse, France

ABSTRACT Using spectroscopic methods, we have studied the structural changes induced in both protein and DNA upon binding of the High-Mobility Group I (HMG-I) protein to a 21-bp sequence derived from mouse satellite DNA. We show that these structural changes depend on the stoichiometry of the protein/DNA complexes formed, as determined by Job plots derived from experiments using pyrene-labeled duplexes. Circular dichroism and melting temperature experiments extended in the far ultraviolet range show that while native HMG-I is mainly random coiled in solution, it adopts a $\beta$-turn conformation upon forming a 1:1 complex in which the protein first binds to one of two dA·dT stretches present in the duplex. HMG-I structure in the 1:1 complex is dependent on the sequence of its DNA target. A 3:1 HMG-I/DNA complex can also form and is characterized by a small increase in the DNA natural bend and/or compaction coupled to a change in the protein conformation, as determined from fluorescence resonance energy transfer (FRET) experiments. In addition, a peptide corresponding to an extended DNA-binding domain of HMG-I induces an ordered condensation of DNA duplexes. Based on the constraints derived from pyrene excimer measurements, we present a model of these nucleated structures. Our results illustrate an extreme case of protein structure induced by DNA conformation that may bear on the evolutionary conservation of the DNA-binding motifs of HMG-I. We discuss the functional relevance of the structural flexibility of HMG-I associated with the nature of its DNA targets and the implications of the binding stoichiometry for several aspects of chromatin structure and gene regulation.

## INTRODUCTION

The High-Mobility Group I (HMG-I/Y) proteins are low-molecular-mass (10.7–11.7 kDa) nonhistone chromosomal proteins that bind to the minor groove of AT-rich DNA without clear sequence specificity (Bustin and Reeves, 1996; Salomon et al., 1986) and recognize noncanonical DNA conformations such as four-way junctions (Hill and Reeves, 1997). HMG-I/Y contains three DNA-binding domains, consisting of 9–10 basic residues, called AT hooks (Bewley et al., 1998, and references cited therein), which are separated by linkers of variable lengths, as well as a short C-terminal acidic domain.

HMG-I was first identified as a factor associated with the $\alpha$-satellite heterochromatin sequences of the green monkey, where it may play a role in nucleosome phasing (Strauss and Varshavsky, 1984). HMG-I binding sites have also been characterized in the related mouse $\alpha$-satellite repeats. These intrinsically curved sequences also contain multiple binding sites for HMG-I, the distribution of which has been compared to known nucleosome phases characterized in vitro (Radic et al., 1987, 1992; Martinez-Balbas et al., 1990; Linxweiler and Hörz, 1985; Carrera et al., 1991; Reeves and Wolffe, 1996). More recently, HMG-I was proposed to play a role in the modulation of chromatin structure and accessibility by antagonizing histone H1 binding to AT-rich scaffold/matrix-associated regions (SARs/MARs) (Zhao et al., 1993; Strick and Laemmli, 1995). It has also been shown to have important functions in the formation of multiprotein complexes, enhancesomes, that regulate the transcription of several genes (Thanos and Maniatis, 1995; Bonnefoy et al., 1999; Du et al., 1993; Mantovani et al., 1998; Yie et al., 1999). Indeed, a number of cytokine genes, such as $\beta$-interferon, interleukin-2 receptor $\alpha$-chain, interleukin-4 receptor, as well as herpes and human papilloma viral genes, are regulated by HMG-I (Thanos and Maniatis, 1995; John et al., 1995, 1996; Kelin-Hessling et al., 1996; French et al., 1996; Kinioshita et al., 1996; Leger et al., 1995). Finally, HMG-I is a critical cellular factor required for the formation of functional HIV-1 preintegration complexes (Li et al., 1998; Farnet and Bushman, 1997), possibly reflecting its role in promoting the assembly of biologically active nucleoprotein complexes. HMG-I is abundant in eukaryotic nondifferentiated cells and in embryos (Bustin and Reeves, 1996; Chiappeta et al., 1996; Amirand et al., 1998), and elevated levels of the protein have been correlated with neoplastic transformation (Holth et al., 1997; Bandiera et al., 1998).

The diverse functions that can be inferred for HMG-I in heterochromatin organization and nucleosome phasing, in the modulation of chromatin structure and in the formation of specialized transcriptional complexes, all ultimately depend on its binding to DNA. Some of these functions might

*Received for publication 8 November 1999 and in final form 10 February 2000.*

Address reprint requests to Dr. Anny Slama-Schwok, INSERM U451, Laboratoire d'Optique Appliquée, Ecole Polytechnique/ENSTA, Palaiseau, France. Tel.: 33-1-43-25-26-09; Fax: 33-1-69-31-99-96; E-mail: schwok@enstay.ensta.fr.



0006-3495/00/05/2543/17 $2.00

be related to protein-mediated structural alterations in the DNA helix, and previous studies have focused on the induction or reversal of DNA bends by HMG-I/Y and on the possibility of inter- or intramolecular cooperative interactions involving multiple AT hooks (Yie et al., 1997; Maher and Nathans, 1996; Falvo et al., 1995; Chase et al., 1999; Lehn et al., 1988; Nissen and Reeves, 1995). However, the nature and the stoichiometry of the complexes that can be formed on a potentially broad set of binding sites have not been studied in detail and remain poorly understood.

We have addressed this question by characterizing the structural changes that are induced in both protein and DNA when HMG-I binds to a DNA fragment of defined sequence and by determining how these changes vary with the stoichiometry of the nucleoprotein complexes that are formed. The results of our studies are consistent with the induction, upon HMG-I binding to DNA, of large conformational changes in the protein that are coupled to relatively small changes in the structure of the DNA duplex, in agreement with the induced-fit model proposed by Record (Spolar and Record, 1994). We present evidence that HMG-I is capable of forming multiple discrete complexes with DNA in which the protein structure varies. The protein conformation and its binding modes are highly sensitive to small changes in DNA sequence, suggesting that HMG-I mainly recognizes DNA structural properties and/or flexibility. Finally, a peptide corresponding to an extended AT-hook motif (Reeves and Nissen, 1990; Geierstanger et al., 1994; Evans et al., 1995) forms ordered DNA aggregates, a property not shared by the full-length protein, which can be fitted by molecular modeling to energetically favorable structures. We discuss the biological implications of our findings in the light of our recent results showing that both HMG-I and ATX promote the onset of zygotic transcription in early mouse embryos (Beaujean et al., manuscript submitted for publication).

## EXPERIMENTAL PROCEDURES

### Materials

Succinimidyl-1-pyrenebutyrate, phosphoramidites, and aminolink 2 reagents were purchased from Molecular Probes and Applied Biosystems. Unlabeled oligonucleotides (Oligold) and high-performance liquid chromatography-purified fluorescein- and rhodamine-labeled oligonucleotides were supplied by Eurogentec. All chemical reagents used were of the highest commercially available purity. The solutions contained 10 mM buffer at pH 7.2 and 50 mM NaCl unless otherwise stated. Piperazine *N, N′*-bis(2-ethanesulfonic acid) (PIPES) was used in most experiments. For thermal denaturation experiments, a cacodylate buffer was used instead because of its lower absorbance. Identical $T_m$ values were obtained at 259 nm with the two buffers.

### Oligonucleotides and peptide

The synthesis and purification of the oligonucleotides labeled at their 5′ end with pyrene (Py) were performed as described (Mohammadi et al., 1997). The fluorescein and rhodamine labels were linked to the oligonucleotides via a hexamethylene (C6) linker. All oligonucleotides were precipitated in ethanol in the presence of NaCl and desalted using Millipore Ultrafree filters with a molecular weight cutoff of 5000. The fluorescein- and rhodamine-labeled oligonucleotides were then extensively washed and reconcentrated in water, using Millipore filters to eliminate all traces of free label. The 21-base (D21, C21) and 39-base (D39) oligonucleotides used in our studies are described in Fig. 1; Py-labeled 11-mers and 21-mers mutated at the AAAT site, which were also used in this work, have the following sequences:

(Py)-11A: 5′ (Py) TAA AAA ACG TG 3′
(Py)-11T: 5′ (Py) CAC GTT TTT TA 3′
(Py)-21$A_1$: 5′ (Py) ACG AGC GCA CTA AAA AAC GTG 3′
(Py)-21$T_1$: 5′ (Py) CAC GTT TTT TAG TGC GCT CGT 3′

The preparation of purified recombinant HMG-I protein was performed as described (Strick and Laemmli, 1995). Protein concentrations were measured by the bicinchoninic acid method as described by the manufacturer (Pierce Chemical Company), using solutions of bovine serum albumin and myoglobin as standards. Alternatively, HMG-I concentrations were determined using $\epsilon = 2.15 \times 10^5$ and $8 \times 10^4$ $M^{-1}$ $cm^{-1}$ in cacodylate and PIPES buffers at 206 and 217 nm, respectively, but these measurements are reliable only above 1.5 $\mu$M because the protein readily adsorbs on the cell walls in the absence of DNA.

The ATX peptide (YGRPKKPRGRPKKGRPKK) was synthesized on an Applied Biosystems (Foster City, CA) 430A synthesizer on HMP resin (Bachem, France). Amino acid side chains were protected by the use of fluorenylmethyloxylcarbonyl (Fmoc) amino acid chemistry. The purity of the peptide (>98%) was assessed by high-performance liquid chromatography (Applied Biosystems 131A) on an Aquapore RP300 column (220/4.6 cm). The integrity of the peptide was further checked by electrospray ionization, using a Finnegan TSQ 700 mass spectrometer, with an observed monoprotonated molar mass of 1971.1 (expected: 1971.4).

### Melting temperature determination

$T_m$ measurements were performed using a Kontron 942 spectrophotometer. The temperature within the cell was measured with a temperature sensor. The melting profiles were monitored at 259, 211, and 222 nm and first corrected for baseline fluctuations by subtracting the absorbance at the same wavelength of a matched cell filled with buffer. Experiments at 211 and 222 nm require thorough monitoring of the apparatus response because the intensity of the deuterium lamp is lower than at 259 nm, and the buffer probably contributes to the absorbance. To do this, the melting profiles of the free DNA duplexes were taken as references and measured at all wavelengths. Any differences between the melting profiles recorded in the far UV, normalized relative to those monitored at 259 nm, were taken as corrections. This procedure was required at wavelengths below 210 nm. Thermal denaturation profiles of protein/DNA complexes were corrected for the contribution of DNA melting to the total absorbance, using the ratio of the absorption in the far UV relative to that at 259 nm (measured at 10°C) and the melting of the same DNA solution monitored at 259 nm. Duplexes were heated to 70°C for 20 min then gently cooled to 10°C and maintained at this temperature overnight before measurement. The melting curve derivatives were obtained with Origin 3.5 software.

### Circular dichroism

Circular dichroism (CD) was measured at 25°C in a Jasco J-710 spectropolarimeter, using a 2-nm bandwidth. CD spectra were averaged over eight scans at 100 nm/min to improve the signal-to-noise ratio. A 0.05-cm path-length quartz cell was used in most cases.

### Fluorescence measurements

Fluorescence measurements were performed using a QuantaMaster QM-1 PTI instrument equipped with a Hamamatsu R928 photomultiplier and a

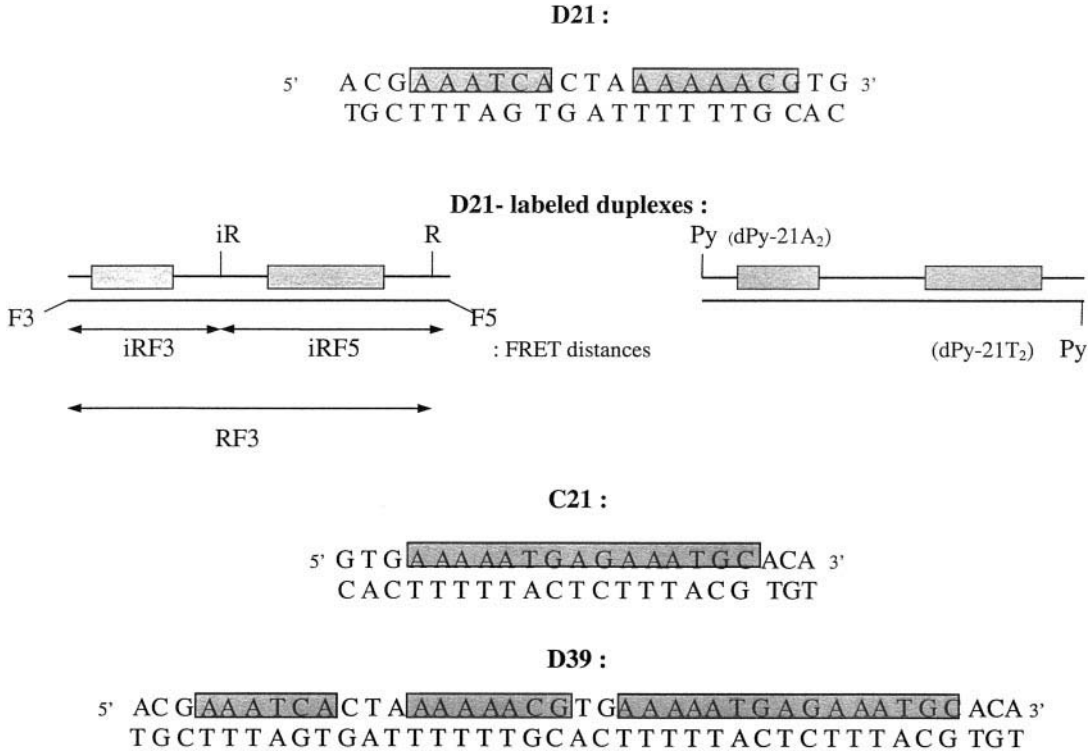


FIGURE 1 Sequences of the D21, C21, and D39 DNA duplexes. Underlined nucleotides represent HMG-I binding sites (Radic et al., 1992; the 5′ and 3′ HMG-I binding sites on the A-rich strand of D21 are arbitrarily referred to in the text as AAAT and $A_6$, respectively, and the numbers are those used in molecular modeling. The position of the labels via a C6 linker to the DNA is schematized by lines. Py stands for pyrene, F for fluorescein, and iR or R for (internal) rhodamine. Each pyrene-linked duplex carries a single label. The sequences of other oligonucleotides used are given in the Experimental Procedures.

thermostatted cell holder. The data collected were corrected for lamp fluctuation, photomultiplier response, and buffer signal. Py-labeled oligonucleotides were usually excited at 348 nm with $\lambda_{em}$ = 360–600 nm, using 2.2- or 3.3-nm slits at the excitation and emission monochromators. Rhodamine-labeled duplexes were excited at 545 and 560 nm, $\lambda_{em}$ = 560/570–700 nm, while fluorescein-labeled duplexes were excited at 480 and 490 nm, $\lambda_{em}$ = 490/500–700 nm. 2.2-nm slits were used in both cases. Samples were prepared for FRET measurements at the acceptor side by dividing into two halves a solution of the rhodamine-labeled strand and adding either the unlabeled or fluorescein-labeled complementary strand, yielding equimolar concentrations of the two strands. Likewise, samples for FRET measurements at the donor side were prepared from the same fluorescein-labeled oligonucleotide solution to obtain the duplexes carrying single or double labels. In addition, FRET measurements from the donor side in the absence of protein were performed with samples prepared differently, as previously described (Toth et al., 1998). The absorbance of the solutions was below 0.04 at the excitation wavelength, thus avoiding inner filter effects. Fluorescence yields were measured using quinine sulfate in 0.1 N sulfuric acid and fluorescein in 0.1 N NaOH as standards (IUPAC, 1986; Sjöback et al., 1995). The oligonucleotides were denatured and renatured as described above, and the complete hybridization of the two strands was assayed by melting temperature measurements. A concentrated stock solution of HMG-I was added stepwise to these DNA duplex solutions.

## Data analysis

The efficiency of Förster energy transfer $E$ between a donor and an acceptor at a distance $R$ is defined as $E = 1/[1 + (R/R_0)^6]$. $R_0$ is the critical distance (expressed in Å) at which $E = 0.5$, $R_0^6 = (8.79 \times 10^{23}) n^{-4} \kappa^2 \phi_D J$, where $n$ is the refractive index of the medium (taken to be 1.4), $\kappa^2$ is the orientation factor, $\phi_D$ is the quantum yield of the donor in the absence of acceptor, and $J$ is the overlap integral between the emission of the donor and the absorption of the acceptor. When energy transfer occurs, the rhodamine (acceptor) emission intensity increases, while that of fluorescein (the donor) simultaneously decreases. The efficiency of energy transfer was calculated from the enhanced acceptor emission and decreased donor emission in three different ways, as follows (Clegg et al., 1993; Jares-Erijman and Jovin, 1996; Toth et al., 1998).

1. The fluorescence spectrum $F_{DA}(490, \lambda_{em})$ of a doubly labeled sample with both fluorescein and rhodamine excited at 490 nm can be fitted by the sum of the two spectral components: the fluorescein emission (singly labeled duplex with fluorescein excited at 490 nm, $F_D(490, \lambda_{em})$) and the enhanced rhodamine emission due to energy transfer (a fraction, ratio $A$, of the signal obtained by direct excitation of the rhodamine at $\lambda$ = 560 nm):

$$F_{DA}(490, \lambda_{em}) = [(a \times F_D(490, \lambda_{em})) + (\text{ratio } A \times F_{DA}(560, \lambda_{em}))].$$

The coefficient $a$ and the ratio $A$ are determined by the fitting procedure. Because rhodamine is also excited directly, albeit to a small extent, at 490 nm, its contribution to the total fluorescence $F_{DA}$ (490, $\lambda_{em}$) is subtracted before the fit. This direct excitation of the acceptor is obtained from the excitation spectrum of the duplex labeled only with rhodamine. The ratio $A$ is related to the energy transfer efficiency as follows:

$$E = E_A = \left[\text{Ratio } A - \frac{\epsilon^A(490)}{\epsilon^A(560)}\right] \times \frac{\epsilon^A(560)}{\epsilon^D(490)}$$

where $\epsilon^A$ and $\epsilon^D$ are extinction coefficients of the donor and the acceptor at a given wavelength, determined from the absorption spectra of the doubly and singly labeled samples.

2. The intensity $F_{DA}$ of the emission of fluorescein in the presence of rhodamine relative to $F_D$, the emission intensity of a duplex carrying a single fluorescein label, is directly related to the energy transfer efficiency $E$ by $E = E_D = 1 - F_{DA}/F_D$. This measurement is straightforward but relies strongly on the presence of identical donor concentrations in both singly and doubly labeled duplexes.

3. The transfer efficiency was also calculated from the normalized ratio of the donor to acceptor emission as defined by Jovin (Jares-Erijman and Jovin, 1996). Briefly, $E_{DA}$ is calculated from emission measurements only: $E = E_{DA} = 1/(1 + (\Phi_A/\Phi_D) \times R_{DA})$, where $R_{DA}$ is the ratio of the fluorescein- to the rhodamine-enhanced emission intensity in the doubly labeled duplex, each of the two terms being normalized by the corresponding emission spectra of the singly labeled duplexes, and $\Phi_A$ and $\Phi_D$ are the fluorescence yields of the acceptor and the donor, respectively.

## Molecular modeling

Molecular modeling was performed with the JUMNA (junction minimization of nucleic acids) program (Lavery et al., 1995). In JUMNA, the efficiency of minimization is improved by the use of helicoidal and internal variables. Individual 3′ nucleotides are positioned with respect to a reference axis system, using helicoidal variables, and their internal flexibility is described by both torsion and valence angles, all bond lengths being fixed. Junctions between successive nucleotides are ensured by quadratic penalty functions. JUMNA uses the Flex force field (Lavery et al., 1995), which is specifically designed for modeling of nucleic acids. Electrostatic damping due to aqueous solvent and counterions is represented by a sigmoidal dielectric function used in calculating electrostatic energy (with a slope of 0.356 and a plateau of 78) and a reduction of the net phosphate charges.

The ATX peptide studied here was constructed with a standard geometry in both an extended conformation and several more compact conformations containing turns. The turns were positioned by scanning the peptide sequence for the tetramer probabilities of $\alpha\alpha$ and $\beta\gamma$ turns as given by Wilmot and Thornton (1990). Eleven conformations corresponding to highest probabilities were constructed and docked with DNA.

Conformations of DNA oligomers, both free and complexed with the ATX peptide, were analyzed using Curves (Lavery and Sklenar, 1989). This program makes it possible to calculate an optimal helical axis (quantitatively describing the curvature of DNA fragment), along with a full set of helicoidal parameters.

## RESULTS

We have studied the interaction of HMG-I with a DNA fragment (between nucleotides 187 and 207) derived from the mouse $\alpha$-satellite repeats that corresponds to one of the largest curvature peaks found in these repeats (Carrera et al., 1991). This 21-bp duplex (D21) contains two AT-rich HMG-I binding sites (Radic et al., 1992): a short AAAT sequence and an $A_6$ tract (Fig. 1). These two sites are separated by 9 bp, close to the ideal phasing required, so that they lie on the same face of the DNA helix. Another duplex, C21, located downstream from the D21 sequence, was also used because it presents similar A-T stretches but in the reverse orientation compared to D21.

The D21 duplex was 5′-end-labeled with pyrene, the fluorescence of which is sensitive to DNA conformation, thus enabling us to monitor the stoichiometry of HMG-I/DNA complexes. Alternatively, the duplex was tagged with rhodamine and fluorescein, allowing us to probe for associated structural changes in the DNA by FRET measurements (Fig. 1). Finally, we performed circular dichroism and melting experiments to detect conformational changes in the protein induced by DNA binding. Most experiments were performed with both HMG-I and a short synthetic peptide, ATX (Amirand et al., 1998; Beaujean et al., 2000), which corresponds to an extended binding domain of the protein (1.5 AT hooks), to characterize those changes dependent on the presence of the three DNA-binding domains of HMG-I and/or of the linkers separating them. Results of these experiments are presented below.

### 1. Denaturation profiles of D21 in the presence of HMG-I and ATX

We first determined the melting profiles of free and bound DNA as a rough measure of the interaction between the protein or the peptide and the duplex. Fig. 2 *A* shows the melting curves of D21 in the absence or presence of HMG-I or ATX. As shown in Fig. 2 *B*, the HMG-I-bound duplex was stabilized relative to free D21 ($\Delta T_m = 13.5 \pm 0.5$°C) in the presence of about one HMG-I molecule per DNA duplex. Higher HMG-I concentrations did not increase the $T_m$ further (Table 1). In contrast, the thermal stabilization of D21 by the ATX peptide was more modest ($\Delta T_m = 10.0 \pm 0.5$°C) and required the presence of a large excess of peptide (Fig. 2 *B*).

### 2. HMG-I and ATX/DNA complex formation monitored by pyrene fluorescence

We sought to characterize HMG-I binding to D21 further by taking advantage of pyrene fluorescence to determine the stoichiometry of the complex(es) formed between DNA and HMG-I or the ATX peptide. Pyrene is a sensitive probe of DNA structure and of local polarity (Rippe et al., 1992; Koenig et al., 1977; Kierzek et al., 1993; Ebata et al., 1995; Mohammadi et al., 1997), and its fluorescence properties might reveal structural changes induced in the DNA by binding of HMG-I. Pyrene should not perturb the duplex because it is uncharged and HMG-I indeed induces a similar stabilization of pyrene-labeled and unlabeled DNA duplexes (see Fig. 2 *B*).

The D21 target DNA contains two distinct binding sites for HMG-I. By linking a pyrene label either at the 5′ end of the A-rich strand close to the AAAT site or at the 5′ extremity of the complementary T strand, in the vicinity of the $A_6$ site, one should be able to distinguish HMG-I binding at each of the two sites in the duplex. We designed two different labeled duplexes, each carrying a single pyrene (Py) probe, dPy-21$A_2$ and dPy-21$T_2$. The positions of the labels are diagrammed in Fig. 1, and the fluorescence prop-

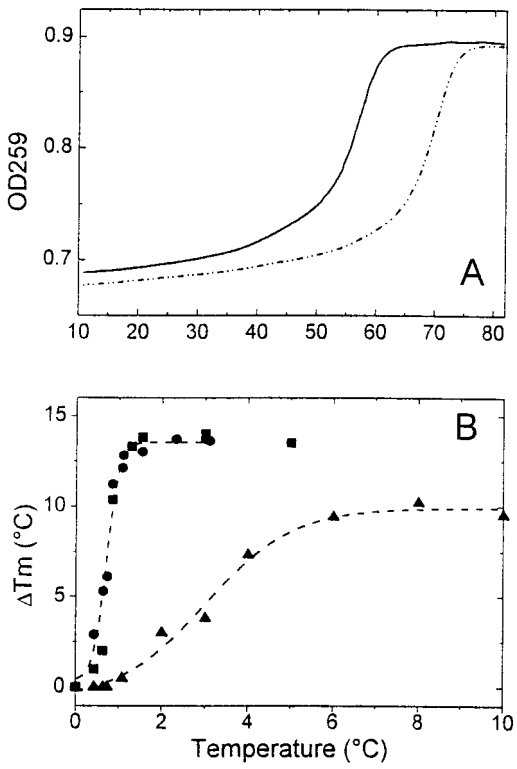


FIGURE 2 Melting profiles of D21 in the absence or presence of HMG-I. Melting curves are shown in *A*. Melting of the D21 duplex was monitored at 259 nm in the absence or presence of 1 HMG-I equivalent (*solid* and *dashed lines*, respectively). (*B*) The variation of the $\Delta T_m = T_m(D21_{bound}) - T_m(D21_{free})$ as a function of HMG-I/DNA or peptide/DNA ratios. Experiments were carried out under the following conditions: [Duplex] = 0.8 $\mu$M, 10 mM cacodylate buffer (pH 7.2), 50 mM NaCl. ■, unlabeled D21; ●, duplex with the Py-21$A_2$-labeled strand in the presence of HMG-I; ▲, D21 in the presence of the ATX peptide.

erties of the Py-labeled duplexes and single-stranded oligonucleotides are summarized in Table 2.

### *Stoichiometry of the HMG-I/DNA and peptide/DNA complexes*

As shown in Fig. 3 *A*, binding of HMG-I to the Py-labeled duplex leads to a large increase in the pyrene fluorescence intensity. This large intensity increase makes it possible to determine the stoichiometry of the protein/DNA complexes by means of Job plots (Loontiens et al., 1990). To do this, we kept the sum of [protein] + [duplex] concentrations constant at 1 $\mu$M, while varying the [duplex]/[protein] ratio. At concentrations that largely exceed the dissociation constant(s), each complex is characterized by a linear dependence of the absorbance or the fluorescence on the concentration, and the stoichiometry is indicated by inflection points.

Fig. 4 *A* shows a representative Job plot derived from an experiment using dPy-21$A_2$, where the difference in the fluorescence intensity of the duplex/HMG-I complexes relative to free dPy$A_2$ was plotted against the mole fraction of duplex given by [dPy-21$A_2$]/([dPy-21$A_2$] + [HMG-I]). Three inflection points can be noted at 0.25 ± 0.02, 0.48 ± 0.04, and 0.84 ± 0.03 mole fraction of duplex. They correspond to three distinct complexes, the stoichiometries of which are 3 HMG-I/duplex, 1 HMG-I/duplex, and 1 HMG-I/~5 duplexes, respectively. We obtained comparable results at higher total concentrations (3 $\mu$M instead of 1 $\mu$M), indicating dissociation constants below the micromolar range (Table 3).

The results of similar experiments performed with the ATX peptide are shown in Fig. 4 *B*. The complexes formed between 0.1 and 0.3 mole fraction of duplex scatter light, introducing some dispersion in the experimental points and a larger uncertainty for the first inflection point. This point, at 0.25 ± 0.05 mole fraction of duplex, corresponds to 3–4 ATX/duplex. The light-scattering properties of this complex are consistent with the formation of aggregates evidenced by the fluorescence data (see below and Section 4). The second inflection point can be more precisely ascertained at 0.50 ± 0.03 mole fraction of duplex and corresponds to a 1:1 peptide/duplex complex, a stoichiometry identical to that of one of the three complexes formed with full-length HMG-I.

### *Comparison of the 5′ and 3′ HMG-I binding sites of the duplex*

As noted above, these experiments, which make it possible to determine the stoichiometry of the protein/DNA complexes, can also be used to ask whether the two binding sites present in the duplex participate equally and/or simultaneously in complex formation. Fig. 3 *A* compares the pyrene fluorescence intensity at 378 nm in the presence of HMG-I relative to the free dPy-21$A_2$ and dPy-21$T_2$ duplexes. Both titration curves reach a plateau at a HMG-I/DNA ratio of 3–4, but their $I/I_0$ limits differ. These curves also differ, at low HMG-I concentrations, by a more rapid increase of the dPy-21$A_2$ fluorescence relative to dPy-21$T_2$.

Fig. 3 *B* presents a similar comparison of dPy-21$A_2$ and dPy-21$T_2$, this time in the presence of the ATX peptide. The increase in pyrene fluorescence was smaller with the peptide than with the protein. A very different response was again observed as a function of the position of the label: binding of the peptide to dPy-21$A_2$ yielded a very small increase in the fluorescence at 378 nm, whereas a sharp transition was observed for dPy-21$T_2$ above 3 ATX peptide equivalents. Surprisingly, at the same peptide concentration, we observed the appearance of a pyrene excimer characterized by a broad emission at 490 nm (Fig. 3 *B*, *inset*). This excimer was absent when dPy-21$A_2$ was used (Table 2 *B*). We verified that these results were not due to nonspecific binding and/or aggregation: in experiments performed in the presence of spermine (up to 12 mM), we could not observe

**TABLE 1 Thermal denaturation parameters determined at 259 and 211 nm**

| [DNA] ($\mu$M) | [HMG-I] ($\mu$M) | [HMG-I]/[DNA] | $T_m$at 211 nm* ($\pm$1°C) | Amplitude† | $T_m$ at 259 nm ($\pm$1°C) |
|---|---|---|---|---|---|
| — | 2–8‡ | — | (20) 60–65 | 1–4 | — |
| — | 13-50ATX§ | — | (18) 60 | 1–3 | — |
| 0.67 | 2 | 3 | (18) 62.7 | 7–8 | 69.9 |
| 1.33 | 2 | 1.5 | 66.7 | 16 | 70.2 |
| 2¶ | 2 | 1 | 70 | 30 | 70.2 |
| 0.67 | — | | 55.8 | | 55.8 |
| 2 | | | 57.1 | | 57.1 |

Results of thermal denaturation experiments performed in 10 mM cacodylate buffer (pH 7.2) and 50 mM NaCl are summarized for D21, HMG-I, and D21/HMG-I complexes.

*Values shown correspond to the maxima of the derivative, assimilated to the $T_m$, while numbers in parentheses refer to shoulders in the curve derivative.

†The amplitude is equal to 100 × (A80-A10)/A10, where A10 and A80 represent the absorbance at 10°C and 80°C, respectively, monitored at 211 nm. The melting curves were corrected by subtracting the DNA contribution at this wavelength for solutions containing both HMG-I and DNA (see Experimental Procedures).

‡Similar $T_m$ values were obtained at 222 nm at HMG-I concentrations ranging from 4 to 16 $\mu$M.

§Note that high peptide concentrations were required to yield conditions comparable to those used with HMG-I in units of peptide bonds.

¶Higher DNA concentrations could not be used at constant [HMG-I] because of excessive total absorbance and the large contribution of the DNA relative to that of the bound protein.

changes in pyrene fluorescence intensity or excimer formation with dPy-21$T_2$ (data not shown).

The presence of an excimer can only result from the close proximity, within 3–5 Å, of at least two DNA duplexes, each carrying a single pyrene label and in parallel orientation relative to one another (Mohammadi et al., 1997, and references therein). If both parallel and antiparallel duplex orientations were possible, one should then observe an excimer with dPy-21$A_2$, which is not the case. These results could thus be explained if the duplexes are organized by the peptide in a parallel orientation starting from a common origin, the $A_6$ binding site present in the duplex, before diverging at distances greater than 5 Å toward the AAAT binding site.

To verify this hypothesis, we synthesized and tested pyrene-labeled 11-mer duplexes, dPy-11A and dPy-11T, bearing only the $A_6$ binding site of the original 21-mer (see Experimental Procedures). Results of these experiments are summarized in Table 2. Addition of the ATX peptide at a concentration of 1 mM induced aggregation of the 11-mer duplexes, with the formation of a large excimer on dPy-11T, similar to that obtained with dPy-21$T_2$. In contrast to dPy-21$A_2$, binding of the peptide to dPy-11A led to an excimer formation, but of half the intensity of the dPy-11T one, as expected if the duplexes diverge from a common origin located at the $A_6$ binding site (Table 2 *B*).

Taken together, our fluorescence data strongly suggest that the complexes formed at high effector/D21 ratios differ in the presence of HMG-I from those observed with the ATX peptide. The latter can induce a supramolecular organization of the duplexes into ordered aggregates, which probably results from the vectorial binding of ATX to DNA. This conclusion is supported by the results of molecular modeling experiments presented below.

**TABLE 2 Fluorescence properties of free and HMG-I- or ATX-bound pyrene-labeled duplexes**

| Labeled strand | Φ single strand* | Φ duplex* | Φ duplex-HMG-I* | $I_\infty/I_0$† |
|---|---|---|---|---|
| A. Labeled duplexes +/− HMG-I | | | | |
| Py-21$A_2$ | $2.0 \times 10^{-2}$ | $4.2 \times 10^{-3}$ | $1.1 \times 10^{-2}$ | (3.0 ± 0.1) |
| Py-21$T_2$ | $2.7 \times 10^{-3}$ | $1.8 \times 10^{-3}$ | $5.0 \times 10^{-3}$ | (3.4 ± 0.1) |

| Labeled strand | $I_\infty/I_0$† | ($I$490/$I$378) ∝‡ |
|---|---|---|
| B. Labeled duplexes/ATX complexes | | |
| Py-21A2 | (1.40 ± 0.05) | 0 |
| Py-21T2 | (2.25 ± 0.07) | (0.23 ± 0.01) |
| | (2.4 ± 0.07)§ | (0.26 ± 0.01)§ |
| Py-21T1 | (3.2 ± 0.1) | (0.16 ± 0.01) |
| Py-11A1 | (1.45 ± 0.05)§ | (0.08 ± 0.01)§ |
| Py-11T1 | (5.4 ± 0.2)§ | (0.21 ± 0.1)§ |

Experiments were performed in 10 mM PIPES buffer (pH 7.2) and 50 mM NaCl at $T$ = 25°C, except where noted§ where T = 20°C; samples were excited at $\lambda$ = 348 nm, using 2 or 3-nm excitation and emission slits. Measured values are shown for free and HMG-I-bound pyrene-labeled duplexes (A) while the properties of ATX-bound labeled DNA are summarized in B.

*The quantum yields were calculated relative to quinine sulfate $\Phi$ = 0.545 in 0.1 N $H_2SO_4$ (IUPAC, 1986). The error on the values is ±6%.

†$I_\infty/I_0$ is the ratio of the pyrene fluorescence intensity measured at $\lambda$ = 378 nm in the presence of a large excess of HMG-I relative to that of the free duplex.

‡Ratio of pyrene excimer to monomer intensities at 490 and 378 nm, respectively, in the presence of a large excess of ATX peptide.

## 3. Structural changes induced in DNA by binding of HMG-I measured by FRET

FRET has been widely used to determine the distance between chromophores bound to a relatively rigid structure, with numerous applications to the fields of nucleic acid structure and protein-DNA interactions (Gohlke et al., 1994;

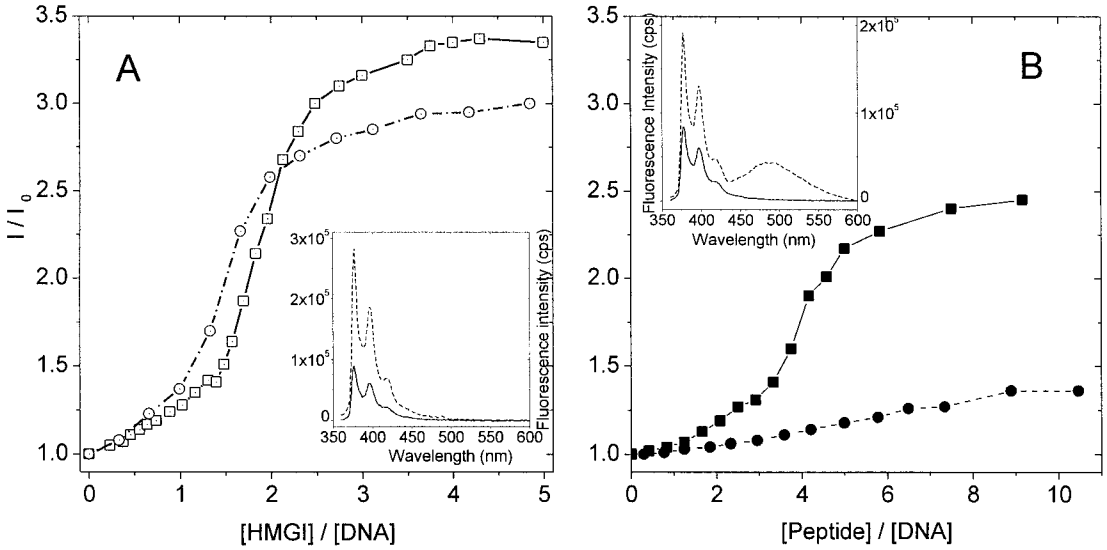


FIGURE 3 Fluorescence changes induced in Py-labeled duplexes by HMG-I and ATX. Conditions are the same as those described in Fig. 2, except that PIPES buffer was used instead of cacodylate. D21 duplexes were labeled with pyrene on either strand (see Fig. 1) and equilibrated with increasing amounts of HMG-I (*A*) or ATX (*B*). The fluorescence intensity *I* measured at 378 nm is normalized to that obtained with the free pyrene-labeled duplex $I_0$. In each panel, dPy-21$A_2$ is represented by circles, dPy-21$T_2$ by squares. The insets show fluorescence spectra of the free (*bottom curves*), HMG-I-bound dPy-21$A_2$ and ATX-bound dPy-21$T_2$ duplexes (*upper curves*) excited at 348 nm.

Clegg et al., 1993; Eis and Millar, 1993, Mergny et al., 1991; Jares-Erijman and Jovin, 1996; Heyduk et al., 1997; Toth et al., 1998). We used FRET to compare interchromophore distances in the absence or presence of HMG-I, using fluorescein and rhodamine as the donor and acceptor, respectively. Rhodamine was either linked to T11 or T20 of the A-rich strand, while fluorescein was introduced at the 5′ or 3′ end of the complementary strand. This defines three donor-acceptor distances (see Fig. 1). The first donor-acceptor pair flanks the short AAAT site (iRF3), the second one spans the long $A_6$ site (iRF5), and the third one is close to the end-to-end distance of the duplex (RF3).

We first verified the feasibility of using these labeled DNA molecules. Control experiments showed that the internal rhodamine label at T11, although it slightly modified the CD spectrum relative to the unlabeled duplex, yielded a comparable difference spectrum (see Fig. 7 *A* and data not shown). In addition, the labeling did not change the thermal

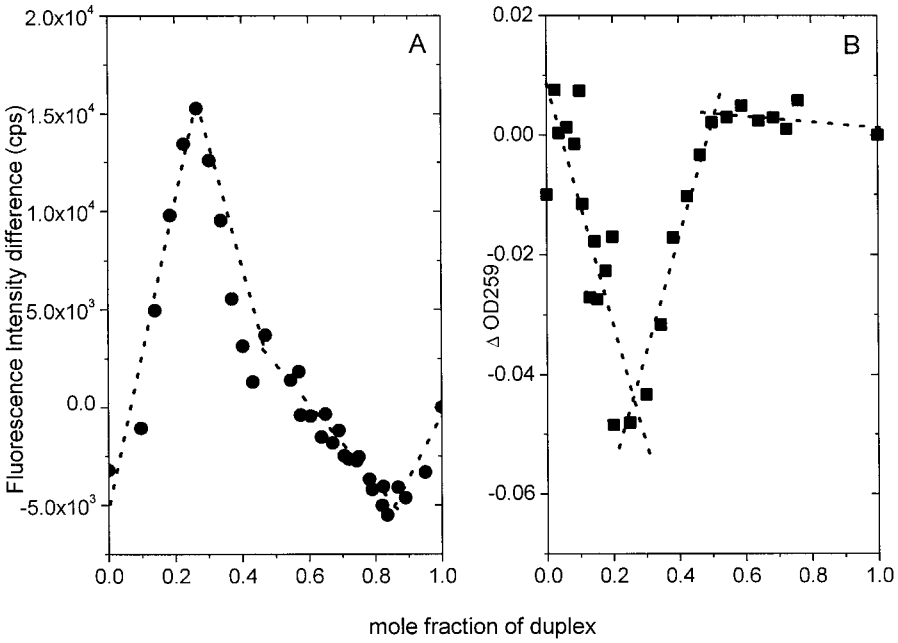


FIGURE 4 Job plots of Py-labeled D21 in the presence of HMG-I or ATX. Job plots of dPy-21$A_2$ in the presence of HMG-I are shown in *A*. Fluorescence signals were obtained using [duplex] + [HMG-I] = 1 $\mu$M, $\lambda$exc = 348 nm, and $\lambda$em = 378 nm. (*B*) [duplex]+ [ATX] = 1 $\mu$M. Absorbance changes were monitored at 259 nm. Note that because ATX induces small fluorescence changes at low concentrations, the absorbance is more sensitive to changes in the stoichiometry. 10 mM PIPES buffer (pH 7.2), 50 mM NaCl.

**TABLE 3 Stoichiometry of the complexes formed by HMG-I or ATX with DNA as obtained from Job plots**

| Complex | Inflection abs mole fraction* | Inflection fluo mole fraction† | Stoichiometry HMG-I/duplex | Stoichiometry ATX/duplex |
|---|---|---|---|---|
| [dPy21$A_2$] + [HMG-I] = 1 $\mu$M | | 0.25 ± 0.02 | 3–4 | |
| | 0.55 ± 0.04 | 0.48 ± 0.04 | 1 | |
| | 0.82 ± 0.03 | 0.84 ± 0.03 | 0.2 | |
| [dPy21$T_2$] + [HMG-I] = 3 $\mu$M | 0.24 ± 0.02 | | 3 | |
| | 0.50 ± 0.04 | | 1 | |
| | 0.77 ± 0.03 | | 0.3 | |
| [dPy21$A_2$] + [ATX] = 1 $\mu$M | 0.22 ± 0.04 | 0.18 ± 0.04 | | 3–4 |
| | 0.50 ± 0.03 | 0.50 ± 0.03 | | 1 |
| [dPy21$T_2$] + [ATX] = 4 $\mu$M | | 0.17 ± 0.04 | | 6–7 |
| | 0.25 ± 0.05 | 0.25 ± 0.05 | | 3 |
| | 0.50 ± 0.03 | 0.50 ± 0.03 | | 1 |

Experiments were performed in 10 mM PIPES buffer (pH 7.2) and 50 mM NaCl.
*Absorption changes monitored at 259 nm.
†Fluorescence changes recorded at 378 nm upon excitation at $\lambda$ = 348 nm, using 2-nm slits.

stabilization of the three labeled duplexes by HMG-I relative to D21 (data not shown). Thus the introduction of the chromophores does not perturb the duplex-HMG-I interactions, validating FRET as a tool for the study of local DNA structural changes induced by HMG-I binding.

Energy transfer efficiency $E$ is calculated from the enhanced acceptor emission $E_A$, the decreased donor fluorescence $E_D$, and the ratio of donor to acceptor $E_{DA}$ (Clegg et al., 1993; Jares-Erijman and Jovin, 1996; Toth et al., 1998). Fig. 5 *A* shows plots of $E$ as a function of added HMG-I, in which each point was derived from the values of $E_A$, $E_D$, and $E_{DA}$ calculated from two independent measurements, with an error of 0.01 (see Experimental Procedures). We first examined changes in energy transfer for the donor-acceptor pair spanning the AAAT site: upon addition of HMG-I to the duplex, the efficiency increased from 0.47 to 0.56 in the presence of two protein molecules per DNA, then leveled off. In contrast, the energy transfer for the donor-acceptor pair spanning the $A_6$ site first reached an apparent plateau at a ratio of two HMG-I per DNA, then leveled off at three HMG-I equivalents. Finally, the end-to-end donor-acceptor pair first exhibited an energy transfer increase after the addition of one HMG-I equivalent, followed by another increase between two and three HMG-I molecules added per duplex.

The resulting donor-acceptor distances are shown (Fig. 5 *B*); they correspond to the data of Fig. 5 *A*, using a random orientation factor $\kappa^2$ = 0.66 and $R_0$ = 51.7 Å which corresponds to a mean value, obtained for RF3, iRF3, and iRF5, ranging between 50.7 ± 0.4 and 52.7 ± 0.4 Å in the absence and presence of a large HMG-I excess relative to DNA, respectively. These results show that the interchro-

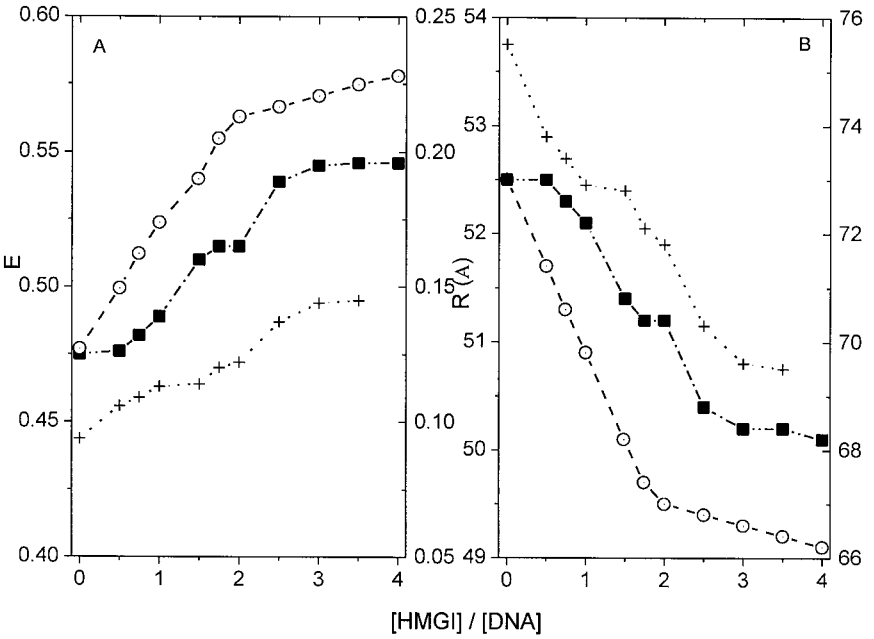


FIGURE 5 Fluorescence energy transfer observed in the presence of HMG-I. (*A*) Transfer efficiency $E$ as a function of the HMG-I/DNA ratio. Each point represents the average of $E_A$, $E_D$, and $E_{DA}$ values from two experiments using the different duplexes described in Fig. 1. iRF3 is represented by circles and iRF5 by squares (*left scale*). RF3 is represented by crosses (*right scale*). (*B*) Corresponding distances, using $R_0$ = 51.7 Å and $\kappa^2$ = 0.66 (random orientation).

mophore distance spanning the short AAAT site decreases by up to ~3.5 Å in the presence of HMG-I, whereas the distance corresponding to the longer $A_6$ site decreases by only 2.5 Å. Correspondingly, the donor-acceptor pair separated by the 19 base pairs that span the two binding sites is brought 6.0 ± 0.8 Å closer in the presence of excess HMG-I. This holds true at protein/DNA ratios of 3:1 to 4:1, corresponding to the formation of the 3:1 protein/DNA complex. The 1:1 complex is characterized by a small distance change, $\Delta R \cong 1.5$ Å, at the AAAT binding site (iRF3), while the $A_6$ site (iRF5) undergoes a negligible change compared to the protein-free duplex. The donor-acceptor pair spanning the two binding sites (RF3) yields an distance change of $\Delta R \cong 1.7$ Å, corroborating this assignment.

These results show that the two binding sites contained in the DNA fragment used are not equivalent and that the shorter AAAT site is occupied by HMG-I first. HMG-I increases the intrinsic curvature and/or shortens the length of the 21-mer duplex upon formation of the 3:1 complex.

## 4. Structural modifications revealed by CD spectroscopy

### *Free protein and peptide*

We sought additional evidence for conformational changes induced in both HMG-I and the DNA duplex upon formation of the different complexes described above. To do this, we first analyzed the CD spectra of the protein in the absence of DNA. Free HMG-I and the ATX peptide both exhibit a strong negative band at 200 nm and a shoulder around 225 nm (Fig. 6 *A*, *spectrum a*, and data not shown). The intensity of the ellipticity was proportional to protein concentration, suggesting that the protein is monomeric in the 4–25 μM concentration range. Finally, the HMG-I spectrum did not show the typical CD signature of an α-helix, even in the presence of 10% trifluoroethanol, a conformation possibly precluded by the proline and glycine residues of the AT hooks (Kentsis and Sosnick, 1998; Tan and Frankel, 1995). The HMG-I CD spectrum fitted a random-coil content of 73 ± 6% and a β-turn content of 27 ± 6%. This fit should be considered together with the $T_m$ data presented below.

### *HMG-I/DNA complexes*

The CD spectrum of the D21 duplex is characterized by peaks at 280 and 220 nm and a negative band at 249 nm, characteristic of DNA in B conformation (Fig. 6 *A*, *spectrum b*). The interaction of HMG-I with the D21 duplex occurs in two distinct steps (Fig. 6 *A*, *bottom panel*). An isoelliptic point is observed at 264 nm. A difference spectrum can be calculated by subtracting the sum of the free HMG-I and duplex spectra from that measured for the 1:1

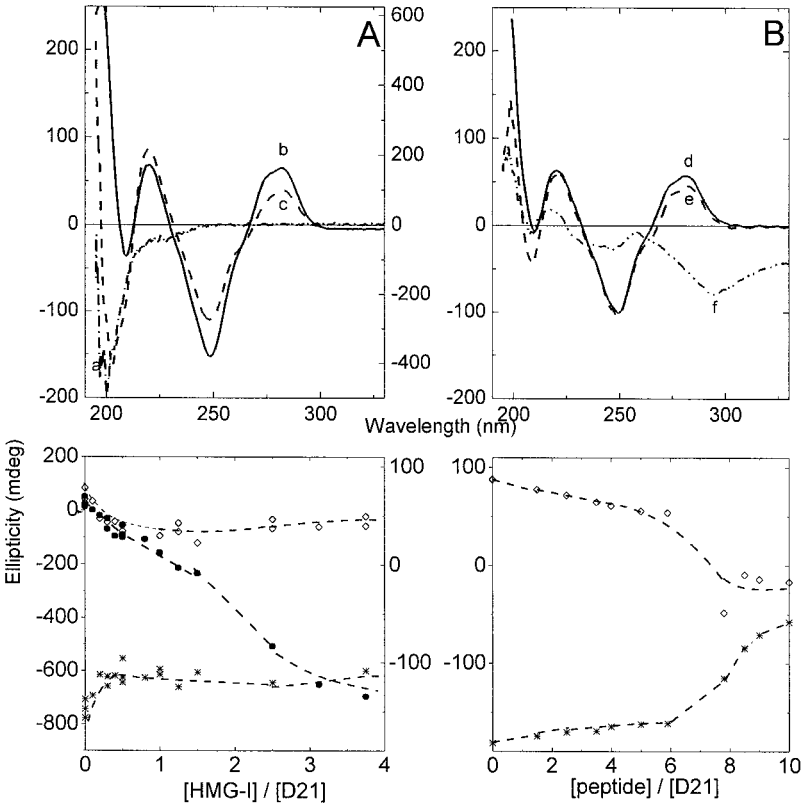


FIGURE 6 CD spectra of free and bound D21, HMG-I, and ATX peptide. Experiments were performed in PIPES buffer as described above. The CD spectra of HMG-I (16 μM, *spectrum a, right scale*), D21 (16 μM, *spectrum b, left scale*), and HMG-I/D21 (16 μM each, *spectrum c, left scale*), are shown in the upper part of *A*. The spectra are normalized to an optical path length $l$ = 1 cm. The spectra of free D21 (16 μM, *spectrum d*) or D21 complexed with ATX (48 and 60 μM, *spectra e* and *f*, respectively) are shown in the upper part of *B* (normalized to $l$ = 1 cm). The lower part of each panel shows the ellipticity obtained at selected wavelengths as a function of HMG-I or ATX equivalents added. In *A*, measurements at 205 nm are denoted by filled circles (*left scale*), and asterisks and open diamonds correspond to λ = 249 and 280 nm, respectively (*right scale*). In *B*, asterisks and open diamonds represent measurements taken at 249 and 280 nm, respectively. The lower panels have been normalized to $l$ = 1 cm.

HMG-I/D21 complex: this difference spectrum yields a positive peak at 200–205 nm with a shoulder around 220 nm (Fig. 7 *A*, *spectrum a*). By comparison with standard spectra (Yang et al., 1986), this peak is consistent with a 20–40% increase of the $\beta$-turn content compared to the free protein. Note that the difference spectra obtained at HMG-I/DNA protein ratios above 1.5 had a smaller amplitude than at the 1:1 ratio (data not shown).

We next asked whether binding of HMG-I to DNA might depend on the length of the DNA used and/or on the sequence of its two HMG-I binding sites. To address this question, we repeated our experiments, using two different DNA fragments, C21 and D39 (Fig. 1). C21 corresponds to a 21-bp duplex located downstream of the D21 sequence in the mouse satellite repeats. It also contains two HMG-I binding sites but gives rise to a single uninterrupted HMG-I footprint, in contrast to the two distinct footprints reported for D21 (Radic et al., 1992). D39 corresponds to a longer 39-bp fragment that contains the D21 and C21 sequences in tandem, allowing us to compare the formation of HMG-I/DNA complexes on different binding sites, analyzed individually or when they are present on the same DNA molecule.

Fig. 7 *A* shows a comparison of the $\Delta\theta$ difference spectra obtained from C21 and D21. In the absorption range of DNA, the difference spectrum of the C21/HMG-I complex (*curve b*) is comparable to that observed with D21 (*curve a*). However, in the 200–220-nm range, the ellipticity changes in the complexes formed with D21 and C21 are markedly different. This difference is consistent with the hypothesis that the complexes formed by HMG-I with D21 and C21 are distinct, as already suggested by footprinting analysis. Interestingly, the difference spectrum of D39 in this region is similar to that of C21 at HMG-I/DNA ratios close to 1:1 but resembles that of D21 at the higher protein/DNA ratio (Fig. 7, compare *A* and *B*). However, in the DNA region, the $\Delta\theta$ values obtained with D39 are much larger than those obtained in the presence of D21. Finally, the plot of the ellipticity values at 249 nm as a function of the HMG-I/DNA ratio shows two transitions (see Fig. 7 *B*, *inset*). These results suggest that HMG-I first binds to the C21 sequence before binding to the D21 sequence in the larger D39 duplex containing both.

Taken together, these results are consistent with a structuring of the protein upon DNA binding. Analysis of the CD spectra shown here indicates that this induced structuring occurs in parallel to conformational changes in the DNA duplex and depends upon the protein/DNA ratio as well as on the duplex sequence and length, that is, on the nature of the binding sites present in the DNA. This latter conclusion is confirmed by the results of melting experiments presented in Section 5.

### *ATX/D21 complexes*

We also compared the complexes formed by the ATX peptide with D21. Based on the results presented above, the structure—or lack thereof—of ATX resembles that of full-length HMG-I. A comparison of spectra d and e of Fig. 6 *B* shows that, qualitatively, binding of the peptide yields changes in the structure of the D21 duplex that are similar to those induced by full-length HMG-I. However, we did not observe, in the peptide absorption region, a difference spectrum similar to that shown in Fig. 7 *A* for the full-length protein. The presence of a large excess of peptide relative to D21 induced an inversion and a shift of the 280-nm band, as well as a decrease in the negative 249-nm and positive 225-nm bands (Fig. 6 *B*, *spectrum f*). High concentrations of

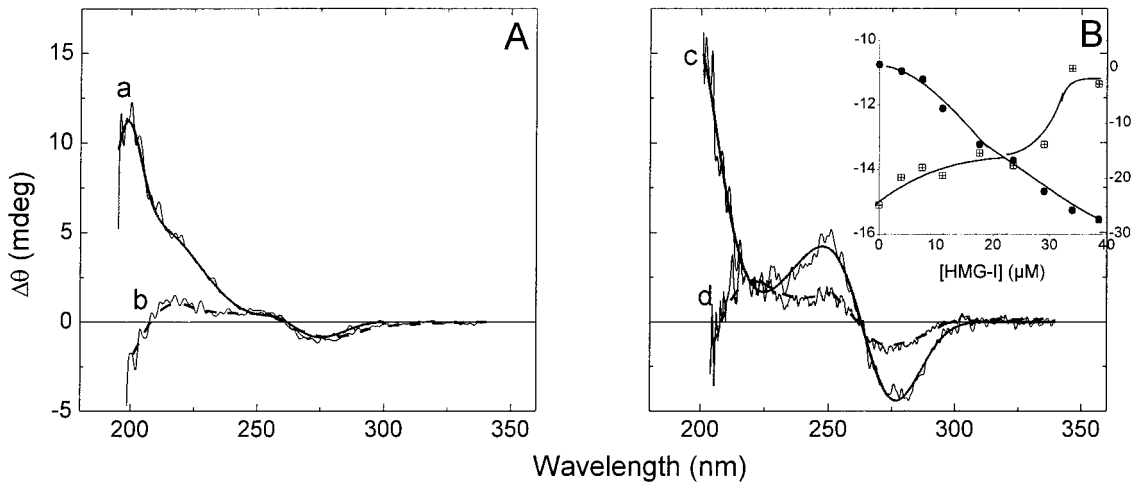


FIGURE 7 Difference CD spectra of HMG-I bound to different DNA duplexes. Experimental conditions are as described in the legend to Fig. 6. (*A*) One equivalent of HMG-I bound to 16 $\mu$M D21 (*spectrum a*) or C21 (*spectrum b*). The $\Delta\theta$ spectra of D39 (16 $\mu$M) at HMG-I/DNA ratios of 1.2 (*spectrum d*) and 2.75 (*spectrum c*) are shown in *B*; the inset shows the ellipticity values of D39/HMG-I complexes monitored at 205 (*circles, right scale*) and 249 nm (*squares, left scale*) as a function of the protein concentration.

spermine or of polylysine, as well as basic peptides derived from histone H1, are known to produce an inversion of the 280-nm band, which was attributed to the formation of $\Psi^-$ aggregates (Khadake and Rao, 1997; Bailly et al., 1993; Erard et al., 1990; Maestre and Reich, 1980; Gosule and Schellman, 1978). Although the amplitude of the negative signal reported in these cases is much larger than that observed with the ATX peptide, it is likely that the peptide, which carries 10 positive charges, induces DNA aggregation when present at concentrations close to those required to neutralize the negative charges of the D21 duplex. These results are thus in excellent agreement with the fluorescence data showing the appearance of an excimer, indicative of a supramolecular organization of the DNA duplex induced by binding of ATX (Fig. 3 *B*), as modeled in Section 6.

## 5. Melting profiles of free HMG-I, ATX peptide, and HMG-I bound to D21

The results of the CD experiments presented above suggest that HMG-I is most likely largely unstructured in solution but undergoes structural changes upon formation of a complex with duplex DNA. To determine whether this is indeed the case, we performed melting experiments extended into the far ultraviolet range, where light absorbance is mainly due to the protein. At 10°C, HMG-I displays an absorption peak at $\lambda_{max} = 206$ nm in cacodylate buffer. At 80°C, this maximum is red-shifted to 211 nm, and a decrease in the absorbance parallels this $\lambda_{max}$ shift. We made use of this phenomenon to monitor possible structural modifications of HMG-I upon heating in the absence or presence of DNA and at different protein/DNA ratios (see Experimental Procedures). We obtained fully reversible denaturation profiles of free and DNA-bound HMG-I.

As shown in Fig. 8, free HMG-I presents a weak absorption transition at ~60°C. This transition is independent of the HMG-I concentration in the range tested (2–16 $\mu$M) and therefore most likely corresponds to an intramolecular folding-unfolding process. We also measured the thermal denaturation of the ATX peptide. Within the limits of experimental error, the peptide melting curve was identical to that of the full-length protein.

In contrast, the extent of protein denaturation was larger in the presence of DNA and, in this case, strongly dependent on the protein/DNA ratio. At a 1:1 protein/DNA ratio (*curve b* in Fig. 8 and see below), the derivative of the denaturation curve of the bound protein showed a sharp peak at 70°C, 10°C higher than the free protein, with small inflections near 50° and 65°C. The presence of these apparent shoulders indicates that the thermal denaturation of HMG-I does not follow a simple two-state model. Consequently, the corresponding van't Hoff values of $\Delta H$ and $\Delta S$ could not be calculated. Results of these experiments, which are summarized in Table 1, also show a decrease of the $T_m$ value when the protein/DNA ratio is increased. This suggests that the protein molecules present in excess relative to DNA are less structured than the first HMG-I equivalent that is bound.

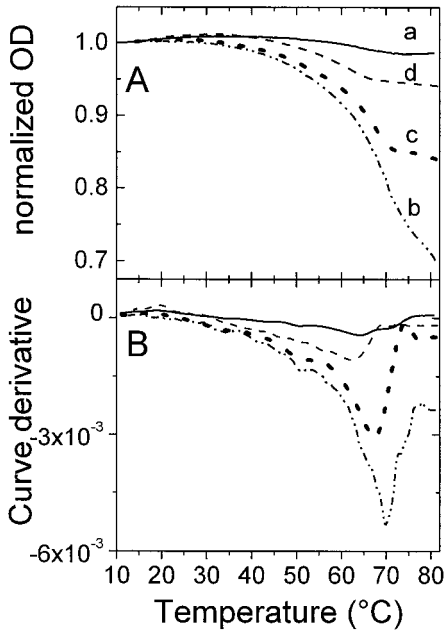


FIGURE 8 Melting curves of free and DNA-bound HMG-I. Melting curves (*A*) and corresponding curve derivatives (*B*) are shown for the free protein (*a*) or for the protein bound to D21 (*b–d*). The absorbance was monitored at 211 nm, where both HMG-I and DNA absorb, and corrected for DNA absorption as detailed in the Experimental Procedures. Melting profiles were determined at HMG-I/DNA ratios of 1:1, 1.5:1, and 3:1 (*curves b, c,* and *d*, respectively). Conditions are as described in Fig. 2.

Our results show that the denaturation/renaturation of both the DNA duplex and the protein are fast relative to the time scale of these experiments. Free HMG-I is as structured (or unstructured) as the ATX peptide. Binding of the protein to the DNA duplex stabilizes both protein and DNA against thermal denaturation. The markedly different melting profiles obtained at protein/DNA ratios ranging from 1:1 to 3:1 clearly show that this transition is dependent on the binding stoichiometry, in agreement with the assignments based on our measurements of changes in pyrene fluorescence upon formation of these complexes (Figs. 3 and 4).

## 6. Molecular modeling of ATX complexes formed with D21 and C21

While the complexes we propose for the interactions between HMG-I and ATX with DNA are based on the experimental data, an important question is whether they correspond to energetically plausible molecular models. We therefore carried out a molecular modeling study based on the JUMNA (junction minimization of nucleic acids) program (Lavery et al., 1995; see the Experimental Procedures for details). The HMG-I protein is too unstructured to en-

able us to carry out a reliable modeling study. Although the ATX peptide represents a simpler case, its lack of secondary structure when uncomplexed again makes modeling difficult. We have therefore focused our study on the conformational aspects of its complexes with DNA. From an energetic point of view it is possible to compare different locations of the ligand bound to DNA as well as different ligand orientations, the energy of the free ligand being a constant term that can be ignored. We were primarily interested in determining whether the difference observed in the interaction of the peptide with the two distinct DNA oligomers, D21 and C21, had its origin in qualitative conformational differences between these two sequences.

The energy-minimized conformations of the two free C21 and D21 oligomers were found to be very similar, exhibiting all the features of a classical B-DNA conformation. Both sequences have an average rise of 3.4 Å and an average twist of 37°, and all of the sugars are positioned in the southern region. There are, however, small differences in helicoidal parameters correlated with the two sequences: base pair inclination is stronger in the vicinity of GC bases pairs, and a strong propeller (10°-30°) is seen for AT bases pairs. Both oligomers are only weakly curved: 17° in the case of D21 and 26° for C21.

### *ATX/D21complex*

The most energetically favorable complex obtained for the ATX peptide bound to D21 is presented in Fig. 9 *A*. In agreement with the preference observed experimentally, the peptide is located on the minor groove side of the $A_6$ tract. This location is significantly more stable than for complexes formed on the AAAT site, though the latter is the preferred binding site for the protein. The geometry of the optimized complex is similar to that of the HMG-I(Y) binding domain bound to the PRDII sequence studied by Huth et al. (1997). In particular, we found the same orientation of the peptide with respect to DNA. Our calculations show that this orientation is favored by both electrostatic and van der Waals interaction energies. The complex shown in Fig. 9 *A* is stabilized by several hydrogen bonds between the peptide and atoms of bases in the minor groove at A14(N3), A15(O1′), and T34(O2), as well as by a series of hydrogen bonds between the anionic oxygens of phosphates 11, 12, 14, 16, and 18 and the cationic side chains of lysines and arginines belonging to ATX. The peptide does not follow the axis of the DNA minor groove, but rather stays on one side of the double helix, also contacting the anionic oxygens of phosphates 17 and 18 on the major groove side. The internal conformation of the peptide is also stabilized by intrapeptide hydrogen bonds of the 1–3 type at its C-terminal end (Arg-8–Arg-10, Lys-12–Lys-14, and Pro-16–Pro-18). Complexation by the ATX peptide does not introduce important conformational changes in the D21 oligomer: its average rise and twist are unchanged, while its curvature increases only very slightly to 24°.

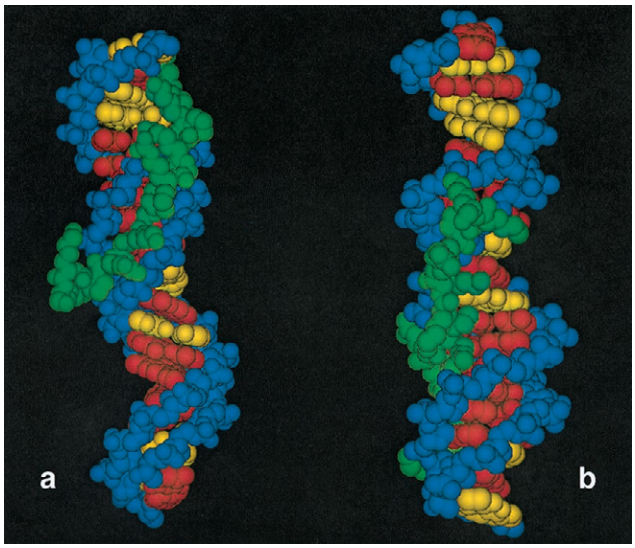


FIGURE 9 Optimal models for the ATX/D21 and ATX/C21 complexes. The energetically most favorable complexes were modeled as detailed in the Experimental Procedures. The ATX/D21 and ATX/C21 complexes are shown in *A* and *B*, respectively. The DNA backbone is colored in blue, AT base pairs in red, and GC base pairs in yellow. The ATX peptide is colored in green.

### *ATX/C21 complex*

In contrast, the lowest-energy complex formed by ATX on C21 has a different location. In this case, the ATX peptide is shifted toward the middle of the oligomer, reaching out to both the AAAT and $A_5T$ sequences. The energy of this complex is weaker than that formed with the D21 sequence. The peptide stays on the outside of the double helix without forming hydrogen bonds to the atoms of the bases, and the curvature of DNA remains unchanged (28°). It is difficult to explain this difference in peptide location, which might be due to a small increase in the curvature of C21 oligomer or, more probably, to differences in the flexibility and in the electrostatic potential and field distributions associated with this particular sequence. While the basis for this difference will have to be addressed in future studies, the model shown in Fig. 9 *B* is consistent with the single uninterrupted HMG-I footprint obtained with the C21 sequence (Radic et al., 1992), in contrast to D21.

### *A model for the ATX/DNA nucleated complex*

We also addressed the question of whether an energetically favorable model might account for the induction of ordered condensation of DNA duplexes by ATX. In this case, the observation of a pyrene excimer suggests that ATX binding to DNA is directional. JUMNA modeling indeed shows that the formation of a complex with two parallel DNA oli-

gomers joined by a single ATX peptide represents an energetically reasonable structure that does not require significant DNA deformations. As shown in Fig. 10, the two DNA oligomers are oriented in a parallel manner and brought together by the ATX peptide bound at the 5′ end of the T-rich strands. In this complex, interactions with the first DNA molecule are almost unchanged, and all of the hydrogen bonds between the ATX peptide and D21 observed in the 1:1 complex are preserved. The same peptide now forms five additional hydrogen bonds to the second DNA oligomer. Formation of this complex does not require important structural adaptations. The first helix is only slightly modified at its 5′ end, and its curvature remains unchanged at 17°. The second helix is somewhat more deformed at the end that contacts the ATX peptide, and its curvature is increased to 37°.

## DISCUSSION

Our work establishes several aspects of HMG-I and ATX structure in solution and upon binding to a short DNA sequence derived from the mouse $\alpha$-satellite repeats that constitute a natural binding site for the protein. We show that HMG-I is capable of undergoing conformational changes as a result of DNA binding. These structural changes depend on the stoichiometry of the HMG-I/DNA complexes formed and on the sequence of the DNA target as detailed below. In contrast, HMG-I or ATX binding induces only minor changes in DNA conformation. We also discuss the relevance of these properties to the functions of HMG-I in vivo.

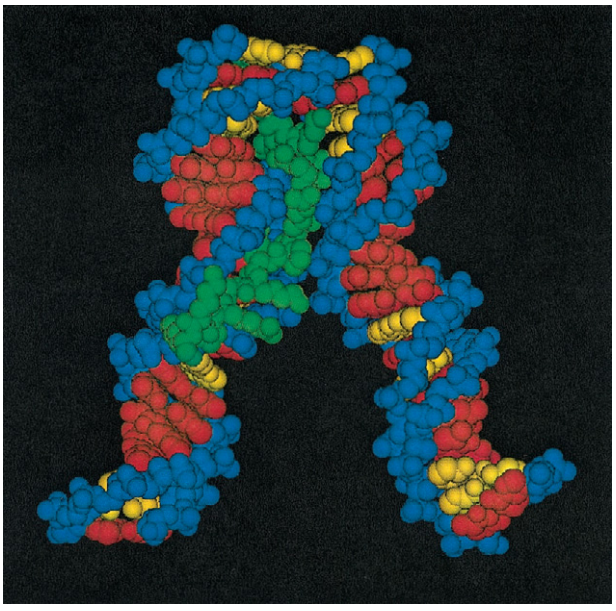

FIGURE 10 A model for the ATX/D21 parallel complex. The complex shown is modeled as described in the legend to Fig. 9. The DNA backbone is colored in blue, AT base pairs in red, and GC base pairs in yellow. The ATX peptide is colored in green. The angle between the two D21 helices is ~45°. The structure obtained accounts for the formation of an ordered 2:1 DNA/ATX complex with two molecules of D21 in parallel orientations and is fully consistent with the presence of the pyrene excimer.

### 1. Free HMG-I is mainly unstructured

The very small amplitude of the protein melting curve shows that, in the absence of DNA, HMG-I is mainly unstructured (Fig. 8). In addition, the CD spectrum of HMG-I is best fitted by ~73% random coil and 27% in $\beta$-turn, the latter probably corresponding to one or more of its AT hooks. Thus the inter-AT hook domains of the full-length protein are probably random-coiled, a conclusion consistent with the suggestion that "in the absence of DNA, the NMR spectrum of HMGI(2/3) (a truncated HMG-I containing two AT hooks) is indicative of random-coiled" (Huth et al., 1997), while a peptide corresponding to one HMG-I AT hook adopts turn-like conformations (Evans et al., 1995).

As our work identifies distinct HMG-I/DNA complexes that differ in their stoichiometries and in the sequences bound, we discuss first the characteristics of each of these complexes before analyzing the structural changes their formation imparts on the protein.

### 2. HMG-I and the ATX peptide form different complexes with the target sequences

HMG-I forms three distinct complexes with the DNA target used: 3:1 and 1:1 protein/DNA complexes and a 1:3–1:5 complex at micromolar concentrations. Preliminary gel retardation assays confirm the existence of 1:1 and 3:1 complexes (data not shown). 1:1 HMG-I/DNA complexes have been reported at low (pM-nM) concentrations (Maher and Nathans, 1996; Reeves and Nissen, 1990). A complex formed by one truncated HMG-I(2/3) molecule per two DNA duplexes has also been reported (Huth et al., 1997). The ATX peptide forms two types of complexes with D21. The first one has a 1:1 stoichiometry and the second one consists of aggregates. Aggregates were reported for an AT hook-derived peptide (Geierstanger et al., 1994), although a single complex was observed with the binding-domain peptide of Reeves and Nissen (1990).

#### *The 1:1 DNA/protein or DNA/peptide complex*

Both HMG-I and ATX both form a well-defined 1:1 complex with DNA, but their respective binding modes depend on the target sequence, D21 or C21. While previous work has shown that a single HMG-I molecule can simultaneously contact two sites in the interferon-$\beta$ promoter and in synthetic sequences (Yie et al., 1997; Maher and Nathans,

1996), our results indicate that this property can be constrained by the DNA sequence.

*HMG-I and ATX bind to a single site of D21.* Our FRET experiments show that, in the 1:1 complex, HMG-I mainly occupies the 5′-most AAAT binding site of D21, which, although shorter than the $A_6$ tract, was indeed predicted to be optimal for HMG-I binding (Huth et al., 1997). Under these conditions, a 21-mer duplex mutated in this site shows an immediate increase of the fluorescence of the Py label linked at the end of the $A_6$ binding site relative to the "delayed" response in 21-d$PyT_2$, where the pyrene is attached at the same end (Fig. 4 *A* and data not shown). This elicits no intramolecular cooperative binding of HMG-I AT hooks to these two sites in the 1:1 complex. The ATX peptide also binds to a single site of D21. The larger and earlier fluorescence increase of d$PyT_2$ compared to d$PyA_2$ (Fig. 3 *B*) suggests that, in this complex, the $A_6$ sequence is favored by ATX over the AAAT binding site, in agreement with the molecular model shown in Fig. 9.

*ATX occupies both AT-rich sites of C21, as reported for HMG-I.* Our results show that the complexes formed by HMG-I on D21 and C21 are different (Fig. 7 *A*), in agreement with footprinting data (Radic et al., 1992; see Fig. 1). ATX follows the same trend: in contrast to its location in the minor groove of D21 (Fig. 9 *A*), ATX remains on the outside of the C21 duplex and reaches out to both the AAAT and $A_5T$ binding sites (Fig. 9 *B*). This may reflect the differences in the intrinsic curvature of D21 and C21 (17° and 26°, respectively), which probably depends on the relative position of the longer $A_6$ or $A_5T$ site with respect to the shorter AAAT one. It seems unlikely that the distance between the two sites, which is similar in D21 and C21, drives these different binding modes (Maher and Nathans, 1996). One possibility is that the two duplexes reach the same final curvature upon formation of the 1:1 complex, in which case the formation of the complex with D21 would be accompanied by a greater deformation or structuring of the protein than when the complex is formed with C21. While it is fully consistent with our CD data, this hypothesis, the corollary of which is that HMG-I recognizes mainly DNA structural properties and/or flexibility, requires additional experimental support.

*Large modification of protein structure coupled to minor DNA structural changes upon 1:1 complex formation.* Our melting experiments show that both the extent of denaturation and the $T_m$ of DNA-bound HMG-I are markedly increased in the 1:1 complex. In parallel, the CD difference spectra observed in the 190–215-nm window, where the protein contributes most of the signal, are similar to that reported for a peptide presenting a type I′ $\beta$-turn (Raghothama et al., 1998). NMR studies of a truncated HMG-I sequence show that the second AT hook forms a type II $\beta$-turn in the minor groove of the DNA (Huth et al., 1997). Thus the spectroscopic changes associated with formation of the 1:1 complex are likely to arise from a restructuring of the DNA-binding domains of the native protein into a $\beta$-turn conformation. In contrast to the large change in protein structure observed upon complex formation, the conformation of the D21 oligonucleotide is only slightly modified, as shown by the results of FRET experiments ($\Delta R \cong 1.7$ Å).

### *The 3:1 multiprotein/DNA complex*

Our study is the first documenting the formation by HMG-I of a single multiprotein/DNA complex with a 3:1 protein/DNA stoichiometry. This complex corresponds to DNA-mediated protein-protein (self) interactions. Protein-protein contacts involving HMG-I have been demonstrated with the bZip and Ets domains of ATF2 and Elf-1 and in the enhancesome (Thanos and Maniatis, 1995; Du et al., 1993; Mantovani et al., 1998; John et al., 1995, 1996). Our FRET data are best explained by the binding of the third HMG-I equivalents to the longer $A_6$ tract. The location of the second protein molecule is less evident because FRET efficiencies are affected at both sites (Fig. 5). A small increase in DNA bending and/or a compaction of the double helix ($\Delta R \cong 4.7$ Å) is associated with HMG-I binding in this complex. This effect is very small compared to the curvature induced by other DNA-binding proteins such as TBP or SRY (Bewley et al., 1998, and references cited therein). In the silencer of the $\beta$-globin gene, binding of HMG-Y results in bending of the DNA (Chase et al., 1999), while it reverses the intrinsic DNA bend of the interferon-$\beta$ enhancer (Falvo et al., 1995). We suggest that HMG-I binding may induce or reverse DNA bending, depending on the sequence context and on the stoichiometry of the complexes formed.

Formation of the 3:1 complex is reflected by a decrease in the CD difference spectrum and in the amplitude and $T_m$ of the protein melting transition (Fig. 8 and data not shown). These differences relative to the 1:1 complex suggest that two of the three HMG-I molecules associated with the 3:1 protein/DNA complex are likely to be much less structured than the first HMG-I equivalent bound. Alternatively, they might adopt different conformations. This new finding of a change in HMG-I structure as a function of the stoichiometry may explain the sensitivity of the pattern of protection of poly d(A-T) against $OH^{\cdot}$ cleavage by HMG-I to the DNA/protein ratio (Franck et al., 1998). Our results suggest that, rather than possessing a preexisting structure that might alter that of DNA, HMG-I can instead adapt its structure upon binding to DNA. This is different from most other DNA binding proteins, for instance the unrelated HMG1 protein, which shares with HMG-I its affinity for the minor groove of AT-rich DNA and its ability to bind to altered DNA structures and to induce DNA bending (Bustin and Reeves, 1996; Hill and Reeves, 1997; Bianchi et al., 1989; Heyduk et al., 1997; Stros, 1998), but has a well-defined structure in solution (Grosschedl et al., 1994). We propose that the adaptability—or induced fit—of HMG-I is

characteristic of an ancillary protein whose binding to different sites might have evolved into different functions. Indeed, a recent report showed that HMG-I-like architectural factors were functional from early in evolution (Aravind and Landsman, 1998). Depending on the context in which they are found, the AT hooks of HMG-I-like proteins might remain independent or interfere with other DNA-binding domains present in these proteins, which would allow for cross-talk to occur between the minor and major grooves of a DNA binding site.

### *Oriented DNA aggregates formed upon ATX binding*

In contrast to the 3:1 HMG-I/DNA complex, ATX forms organized aggregates on D21, as evidenced by CD and fluorescence spectroscopy. These aggregates are oriented and ordered, although the AT-hook motif has been suggested to bind DNA in two orientations (Huth et al., 1997). The energetically reasonable model of this nucleated structure shown in Fig. 10 indeed successfully reproduces the parallel orientation of the two DNA duplexes deduced from pyrene excimer formation. Formation of this structure, which is not seen with the use of full-length HMG-I, does not require important structural changes in the DNA double helices. It is likely that the inter-AT-hook linkers of HMG-I and/or its negatively charged C-terminal domain restrict its binding modes relative to the ATX peptide. Interestingly, MATH20, an artificial protein containing 20 AT-hook motifs connected by linkers, condenses chromatin (Strick and Laemmli, 1995; Girard et al., 1998). This remarkable property suggests that the activity of HMG-I-like proteins can be modulated by the number, spacing, and conformations of their AT-hook motifs.

These multieffector/DNA complexes differ with ATX and HMG-I, although both protein and peptide have been shown to advance the onset of transcription in early mouse embryos (Beaujean et al., in press). Part of the role of HMG-I in the regulation of transcription is to facilitate the formation of multiprotein complexes (Thanos and Maniatis, 1995; Bonnefoy et al., 1999; Du et al., 1993; Mantovani et al., 1998; Yie et al., 1999). However, the ATX peptide does not possess C-terminal or linker domains that would allow the "recruitment" of chromatin remodeling or specific transcription factors, but only an extended AT hook. Thus the finding that ATX can substitute for HMG-I in one-cell mouse embryos is somewhat surprising. Our model of ATX aggregates may provide a clue to this intriguing result. It suggests that the peptide alters the electrostatic field of the DNA at specific sites without major structural rearrangements, allowing closer contact between negatively charged moieties. This may indirectly facilitate protein-protein interactions, even in the absence of a proper protein-binding domain (Panagiotidis et al., 1995). Alternatively, ATX, like HMG-I, may displace factors that inhibit transcription.

## 4. Relevance of the stoichiometry of HMG-I-DNA complexes to HMG-I function in vivo

An important question is whether the complexes characterized in this study can form in vivo. Considerably high local HMG-I concentrations might be found in the nucleus, and HMG-I is indeed known to be concentrated in $\alpha$-satellite repeats. Recently, we have reported the existence of discrete nuclear populations of HMG-I that are highly concentrated relative to the bulk of the protein that is distributed fairly homogeneously within the nucleoplasm (Amirand et al., 1998). We proposed that these subpopulations might reflect distinct and separable biological functions of the HMG-I protein. Furthermore, nucleosome linkers such as those found in AT-rich satellite DNAs or in scaffold-associated regions (SAR/MAR sequences) are greatly enriched for potential HMG-I binding sites. It therefore seems plausible that formation of higher-order complexes might be favored in regions of higher HMG-I local concentrations. If so, one would predict that, under conditions where HMG-I levels decrease, as in the course of development and differentiation, the equilibrium between lower and higher order complexes would be shifted accordingly. Modulation of HMG-I levels would thus provide the means to regulate the stoichiometry—and hence the properties—of the complexes formed at clustered sites—in heterochromatin or at the base of chromatin loops—or at dispersed binding sites in euchromatin.

The authors thank Dr. Jean-Luc Popot for the use of his spectrofluorimeter and Martine Chebrout for excellent technical assistance.

This work was supported by the French Institut National de la Santé et la Recherche Médicale (INSERM), the Centre National de la Recherche Scientifique (CNRS), the Ligue Nationale contre le Cancer, and the Association pour la Recherche sur le Cancer (ARC) (grant 9284 to EK).

## REFERENCES

Amirand, C., A. Viari, J. P. Ballini, H. Rezaei, N. Beaujean, D. Jullien, E. Käs, and P. Debey. 1998. Three distinct sub-nuclear populations of HMG-I protein of different properties revealed by co-localization image analysis. *J. Cell Sci.* 111:3551–3561.

Aravind, L., and D. Landsman. 1998. AT-hook motifs identified in a wide variety of DNA-binding proteins. *Nucleic Acids Res.* 26:4413–4421.

Bailly, F., C. Bailly, P. Colson, C. Houssier, and J. P. Hénichart. 1993. A tandem repeat of the SPKK peptide motif induces $\psi^{-}$type DNA structures at alternating AT sequences. *FEBS Lett.* 324:181–184.

Bandiera, A., D. Bonifacio, F. Mantovani, A. Rustighi, F. Zanconati, A. Fusco, L. Di Bonito, and V. Giancotti. 1998. Expression of HMGI(Y) proteins in squamous intraepithelial and invasive lesions of the uterine cervix. *Cancer Res.* 58:426–431.

Beaujean, N., C. Bouniol-Baily, D. Sullien, K. Kissa, C. Monod, N. Aulner, C. Amirand, P. Debey, and E. Käs. 2000. Induction of early transcription in one-cell embryos by microinjection of the non-histone chromosomal protein HMG-I. *Mol. Dev.* in press.

Bewley, C. A., A. M. Gronenborn, and G. M. Clore. 1998. Minor groove-binding architectural proteins: structure, function, and DNA recognition. *Annu. Rev. Biophys. Biomol. Struct.* 27:105–131.

Bianchi, M. E., M. Beltrame, and G. Paonessa. 1989. Specific recognition of cruciform DNA by nuclear protein HMG1. *Science.* 243:1056–1059.

Bonnefoy, E., M. T. Bandu, and J. Doly. 1999. Specific binding of high-mobility group I (HMGI) protein and histone H1 upstream of the AT-rich region of the murine beta interferon promoter: HMGI protein acts as a potential antirepressor of the promoter. *Mol. Cell. Biol.* 19: 2803–2816.

Bustin, M., and R. Reeves. 1996. High-mobility-group chromosomal proteins: architectural components that facilitate chromatin function. *Prog. Nucleic Acids Res.* 54:35–100.

Carrera, P., A. Martinez-Balbas, and F. Azorin. 1991. Identification of sequence elements contributing to the intrinsic curvature of the mouse satellite DNA repeat. *Nucleic Acids Res.* 19:5639–5644.

Chase, M. B., S. B. Haga, W. D. Hankins, D. M. Williams, Z. Bi, J. W. Strovel, C. Obriecht, and P. E. Berg. 1999. Binding of HMG-I(Y) elicits structural changes in a silencer of the human $\beta$-globin gene. *Am. J. Hematol.* 60:27–35.

Chiappeta, G., V. Avantaggiato, R. Visconti, M. Fedele, S. Battista, F. Trapasso, B. M. Merciai, V. Fidanza, V. Giancotti, M. Santoro, A. Simeone, and A. Fusco. 1996. High level of the HMG I(Y) gene during embryonic development. *Oncogene.* 13:2439–2446.

Clegg, R. M., A. I. H. Murchie, A. Zechel, and D. M. J. Lilley. 1993. Observing the helical geometry of double-stranded DNA in solution by fluorescence resonance energy transfer. *Proc. Natl. Acad. Sci. USA.* 90:2994–2998.

Du, W., D. Thanos, and T. Maniatis. 1993. Mechanisms of transcriptional synergism between distinct virus-inducible enhancer elements. *Cell.* 74:887–898.

Ebata, K., M. Masuko, H. Ohtani, and M. Kashiwasake-Jibu. 1995. Nucleic acid hybridization accompanied with excimer formation from two pyrene-labeled probes. *Photochem. Photobiol.* 62:836–839.

Eis, P. S., and D. P. Millar. 1993. Conformational distributions of a four-way junction revealed by time-resolved fluorescence resonance energy transfer. *Biochemistry.* 32:13852–13860.

Erard, M., F. Lakhdar-Ghazal, and F. Amalric. 1990. Repeat peptide motifs which contain $\beta$-turns and modulate DNA condensation in chromatin. *Eur. J. Biochem.* 191:19–26.

Evans, J. N. S., J. Zajicek, M. S. Nissen, G. Munske, V. Smith, and R. Reeves. 1995. $^{1}H$ and $^{13}C$ NMR assignments and molecular modeling of a minor groove DNA-binding peptide from the HMG-I protein. *Int. J. Pept. Protein Res.* 45:554–560.

Falvo, J. V., D. Thanos, and T. Maniatis. 1995. Reversal of intrinsic DNA bends in the IFN$\beta$ enhancer by transcription factors and the architectural protein HMG I(Y). *Cell.* 83:1101–1111.

Farnet, C. M., and F. D. Bushman. 1997. HIV-1 cDNA integration: requirement of HMGI(Y) protein for function of preintegration complexes in vitro. *Cell.* 88:483–492.

Franck, O., R. Schwanbeck, and J. R. Wisniewski. 1998. Protein footprinting reveals specific binding modes of a high mobility group protein I to DNAs of different conformation. *J. Biol. Chem.* 273:20015–20020.

French, S. W., M. C. Schmidt, and J. C. Glorioso. 1996. Involvement of a high-mobility-group protein in the transcriptional activity of herpes simplex virus latency-active promoter 2. *Mol. Cell. Biol.* 16:5393–5399.

Geierstanger, B. H., B. F. Volkman, W. Kremer, and D. E. Wemmer. 1994. Short peptide fragments derived from HMG-I/Y proteins bind specifically to the minor groove of DNA. *Biochemistry.* 33:5347–5355.

Girard, F., B. Bello, U. K. Laemmli, and W. J. Gehring. 1998. In vivo analysis of scaffold-associated regions in Drosophila: a synthetic high-affinity SAR binding protein suppresses position effect variegation. *EMBO J.* 17:2079–2085.

Gohlke, C., A. I. H. Murchie, D. M. J. Lilley, and R. M. Clegg. 1994. Kinking of DNA and RNA helices by bulged nucleotides observed by fluorescence resonance energy transfer. *Proc. Natl. Acad. Sci. USA.* 91:11660–11664.

Gosule, L. C., and J. A. Schellman. 1978. DNA condensation with polyamines. I. Spectroscopic studies. *J. Mol. Biol.* 121:311–326.

Grosschedl, R., K. Giese, and J. Pagel. 1994. HMG domain proteins: architectural elements in the assembly of nucleoprotein structures. *Trends Genet.* 10:94–99.

Heyduk, E., T. Heyduk, P. Claus, and J. R. Wisniewski. 1997. Conformational changes of DNA induced by the binding of *Chironomus* high mobility group protein 1a (cHMG1a). *J. Biol. Chem.* 272:19763–19770.

Hill, D. A., and R. Reeves. 1997. Competition between HMG-I(Y), HMG-1 and histone H1 on four-way junction DNA. *Nucleic Acids Res.* 25:3523–3531.

Holth, L. T., A. E. Thorlacius, and R. Reeves. 1997. Effects of epidermal growth factor and estrogen on the regulation of the HMG-I/Y gene in human mammary epithelial cell lines. *DNA Cell Biol.* 16:1299–1309.

Huth, J. R., C. A. Bewley, M. S. Nissen, J. N. S. Evans, R. Reeves, A. M. Gronenborn, and G. M. Clore. 1997. The solution structure of an HMG-I(Y)-DNA complex defines a new architectural minor groove binding motif. *Nature Struct. Biol.* 4:657–664.

IUPAC Commission on Photochemistry. 1986. *E. P. A. Newsletter.* 21–29.

Jares-Erijman, E. A., and T. M. Jovin. 1996. Determination of DNA helical handedness by fluorescence resonance energy transfer. *J. Mol. Biol.* 257:597–617.

John, S., R. B. Reeves, J. X. Lin, R. Child, J. M. Leiden, C. B. Thomson, and W. J. Leonard. 1995. Regulation of cell-type-specific interleukin-2 receptor $\alpha$-chain gene expression: potential role of physical interactions between Elf1, HMG-I(Y) and NF-$\kappa$B family proteins. *Mol. Cell. Biol.* 15:1786–1796.

John, S., C. M. Robbins, and W. J. Leonard. 1996. An IL-2 response element in the human IL-2 receptor $\alpha$ chain promoter is a composite element that binds Stat5, Elf-1, HMG-I(Y) and a GATA family protein. *EMBO J.* 15:5627–5635.

Kelin-Hessling, S., G. Schneider, A. Heinfling, S. Chuvpilo, and E. Serfling. 1996. HMGI(Y) interferes with the DNA binding of NF-AT factors and the induction of the interleukin 4 promoter in T cells. *Proc. Natl. Acad. Sci. USA.* 93:15311–15316.

Kentsis, A., and T. R. Sosnick. 1998. Trifluoroethanol promotes helix formation by destabilizing backbone exposure: desolvation rather than native hydrogen bonding defines the kinetic pathway of dimeric coiled coil folding. *Biochemistry.* 37:4613–14622.

Khadake, J., and M. R. S. Rao. 1997. Condensation of DNA and chromatin by an SPKK-containing octapeptide repeat motif present in the C-terminus of histone H1. *Biochemistry.* 36:1041–1051.

Kierzek, R., Y. Li, D. H. Turner, and P. Bevilacqua. 1993. 5′-Amino pyrene provides a sensitive, non-perturbing fluorescent probe of RNA secondary and tertiary structure formation. *J. Am. Chem. Soc.* 115: 4985–4992.

Kinioshita, T., H. Shirasawa, Y. Shino, K. Shimizu, H. Moriya, and B. Simizu. 1996. Human papillomavirus type 16 E6 protein up-regulates the expression of the high mobility group protein HMG-I(Y) gene in mouse 10T1/2 cells. *Virus Res.* 42:119–125.

Koenig, P., S. A. Reines, and C. R. Cantor. 1977. Pyrene derivatives as fluorescent probes of conformation near the 3′ termini of polyribonucleotides. *Biopolymers.* 16:2231–2242.

Lavery, R., and H. Sklenar. 1989. Defining the structure of irregular nucleic acids: conventions and principles. *J. Biomol. Struct. Dyn.* 6:655–667.

Lavery, R., K. Zakrzewska, and H. Sklenar. 1995. JUMNA (junction minimisation of nucleic acids). *Comp. Phys. Commun.* 91:135–158.

Leger, H., E. Sock, K. Renner, F. Grummt, and M. Wegner. 1995. Functional interaction between the POU domain protein Ets-1/Oct6 and the high-mobility-group protein HMG-I/Y. *Mol. Cell. Biol.* 15:3738–3747.

Lehn, D. A., T. S. Elton, K. R. Johnson, and R. Reeves. 1988. A conformational study of the sequence specific binding of HMG-I(Y) with the bovine interleukin-2 cDNA. *Biochem. Int.* 16:963–971.

Li, L., C. M. Farnet, W. F. Anderson, and F. D. Bushman. 1998. Modulation of activity of Moloney murine leukemia virus preintegration complexes by host factors in vitro. *J. Virol.* 72:2125–2131.

Linxweiler, W., and W. Hörz. 1985. Reconstitution experiments show that segment-specific histone-DNA interactions are the basis for nucleosome phasing on mouse satellite DNA. *Cell.* 42:281–290.

Loontiens, F. G., P. Regenfuss, A. Zechel, L. Dumortier, and R. M. Clegg. 1990. Binding characteristics of Hoechst 33258 with calf thymus DNA, poly[d(A-T)], and d(CCGGAATTCCGG): multiple stoichiometries and

determination of tight binding with a wide spectrum of site affinities. *Biochemistry.* 29:9029–9039.

Maestre, M. F., and C. Reich. 1980. Contribution of light scattering to the circular dichroism of deoxyribonucleic acid films, deoxyribonucleic acid-polylysine complexes and deoxyribonucleic acid-particles in ethanolic buffers. *Biochemistry.* 19:5214–5223.

Maher, J. F., and D. Nathans. 1996. Multivalent DNA-binding properties of the HMG-I proteins. *Proc. Natl. Acad. Sci. USA.* 93:6716–6720.

Mantovani, F., S. Covaceuszach, A. Rutighi, R. Sgarra, C. Health, G. H. Goodwin, and G. Manfioletti. 1998. NF-kappa B mediated transcriptional activation is enhanced by the architectural factor HMGI-C. *Nucleic Acids Res.* 26:1433–1439.

Martinez-Balbas, A., A. Rodriguez-Campos, M. Gracia-Ramirez, J. Sainz, P. Carrera, J. Aymami, and F. Azorin. 1990. Satellite DNAs contain sequences that induce curvature. *Biochemistry.* 29:2342–2348.

Mergny, J. L., A. Slama-Schwok, T. Montenay-Garestier, M. Rougée, and C. Hélène. 1991. Fluorescence energy transfer between dimethyldiazaperopyrenium dication and ethidium intercalated in poly d(A-T*). Photochem. Photobiol.* 53:555–558.

Mohammadi, S., A. Slama-Schwok, G. Léger, D. El Manouni, A. Shchyolkina, Y. Leroux, and E. Taillandier. 1997. Triple helix formation and homologous strand exchange in pyrene-labeled oligonucleotides. *Biochemistry.* 36:14836–14844.

Nissen, M. S., and R. Reeves. 1995. Changes in superhelicity are introduced into closed circular DNA by binding of high mobility group protein I/Y. *J. Biol. Chem.* 270:4355–4360.

Panagiotidis, C. A., S. Artandi, K. Calame, and S. J. Silverstein. 1995. Polyamines alter sequence-specific DNA-protein interactions. *Nucleic Acids Res.* 23:1800–1809.

Radic, M. Z., K. Lundgren, and B. A. Hamkal. 1987. Curvature of mouse satellite DNA and condensation of heterochromatin. *Cell.* 50: 1101–1108.

Radic, M. Z., M. Saghbini, T. S. Elton, R. Reeves, and B. A. Hamkalo. 1992. Hoechst 33258, distamycin A, and high mobility group protein I (HMG-I) compete for binding to mouse satellite DNA. *Chromosoma.* 101:602–608.

Raghothama, S., M. Chaddha, S. Banumathi, K. Ravikumar, D. Velmurugan, and P. Balaram. 1998. Conformational interconversions in peptide $\beta$-turns: discrimination between enantiomeric conformations by chiral perturbation. *Biopolymers.* 45:191–202.

Reeves, R., and M. S. Nissen. 1990. The A-T-DNA binding domain of mammalian high mobility group I chromosomal proteins. *J. Biol. Chem.* 265:8573–8582.

Reeves, R., and A. P. Wolffe. 1996. Substrate structure influences binding of the non-histone protein HMG-I(Y) to free and nucleosomal DNA. *Biochemistry.* 35:5063–5074.

Rippe, K., V. Fritsch, E. Westhof, and T. M. Jovin. 1992. Alternating d(G-A) sequences form a parallel-stranded DNA homoduplex. *EMBO J.* 11:3777–3786.

Salomon, M. J., J. F. Strauss, and A. Varshavsky. 1986. A mammalian high mobility group protein recognizes any stretch of six AT base pairs in duplex DNA. *Proc. Natl. Acad. Sci. USA.* 83:1276–1280.

Sjöback, R., J. Nygren, and M. Kubista. 1995. Absorption and fluorescence properties of fluorescein. *Spectrochim. Acta A.* 51:7–21.

Spolar, R. S., and M. T. Record. 1994. Coupling of local folding to site-specific binding of proteins to DNA. *Science.* 263:777–784.

Strauss, F., and A. Varshavsky. 1984. A protein binds to a satellite DNA repeat at three specific sites that would be brought into mutual proximity by DNA folding in the nucleosome. *Cell.* 37:889–901.

Strick, R., and U. K. Laemmli. 1995. SAR are *cis* DNA elements of chromosome dynamics: synthesis of a SAR repressor protein. *Cell.* 83:1137–1148.

Stros, M. 1998. DNA bending by the chromosomal protein HMG1 and its high mobility group box domains. Effect of flanking sequences. *J. Biol. Chem.* 273:10355–10361.

Tan, R., and A. D. Frankel. 1995. Structural variety of arginine-rich RNA-binding peptides. *Proc. Natl. Acad. Sci. USA.* 92:5282–5286.

Thanos, D., and T. Maniatis. 1995. Virus induction of human IFN$\beta$ gene expression requires the assembly of an enhanceosome. *Cell.* 83: 1091–1100.

Toth, K., V. Sauermann, and J. Langovski. 1998. DNA curvature in solution measured by fluorescence resonance energy transfer. *Biochemistry.* 37:8173–8179.

Wilmot, C. M., and J. M. Thornton.1990. $\beta$-Turns and their distortions: a proposed new nomenclature. *Protein Eng.* 3:479–493.

Yang, J. T., C. S. Wu, and H. M. Martinez. 1986. Calculation of protein conformation from circular dichroism. *Methods Enzymol.* 130:208–269.

Yie, J., S. Liang, M. Merika, and D. Thanos. 1997. Intra- and intermolecular cooperative binding of high mobility group protein I(Y) to the beta-interferon promoter. *Mol. Cell. Biol.* 17:3649–3662.

Yie, J., M. Merika, N. Munshi, G. Chen, and D. Thanos. 1999. The role of HMG I(Y) in the assembly and function of the IFN-$\beta$ enhanceosome. *EMBO J.* 18:3074–3089.

Zhao, K. E., E. Käs, E. Gonzalez, and U. K. Laemmli. 1993. SAR-dependent mobilization of histone H1 by HMG-I/Y in vitro: HMG-I/Y is enriched in H1-depleted chromatin. *EMBO J.* 12:3237–3247.